

Article

# Real-Time Approximate Equivalent Consumption Minimization Strategy Based on the Single-Shaft Parallel Hybrid Powertrain

Penghui Qiang, Peng Wu, Tao Pan and Huaquan Zang \*

Institute of Electrical Engineering, Yanshan University, Qinhuangdao 066004, China; ph\_qiang@163.com (P.Q.); pengwu1106@163.com (P.W.); pt\_986@163.com (T.P.)

\* Correspondence: hqzang@hotmail.com

**Abstract:** Real-time energy management strategy (EMS) plays an important role in reducing fuel consumption and maintaining power for the hybrid electric vehicle. However, real-time optimization control is difficult to implement due to the computational load in an instantaneous moment. In this paper, an Approximate equivalent consumption minimization strategy (Approximate-ECMS) is presented for real-time optimization control based on single-shaft parallel hybrid powertrain. The quadratic fitting of the engine fuel consumption rate and the single-axle structure characteristics of the vehicle make the fitness function transformed into a cubic function based on ECMS for solving. The candidate solutions are thus obtained to distribute torque and the optimal distribution is got from the candidate solutions. The results show that the equivalent fuel consumption of Approximate-ECMS was 7.135 L/km by 17.55% improvement compared with Rule-ECMS in the New European Driving Cycle (NEDC). To compensate for the effect of the equivalence factor on fuel consumption, a hybrid dynamic particle swarm optimization-genetic algorithm (DPSO-GA) is used for the optimization of the equivalence factor by 9.9% improvement. The major contribution lies in that the Approximate-ECMS can reduce the computational load for real-time control and prove its effectiveness by comparing different strategies.

**Keywords:** real-time energy management strategy; single-shaft parallel hybrid powertrain; computational load; approximate-ECMS; DPSO-GA



**Citation:** Qiang, P.; Wu, P.; Pan, T.; Zang, H. Real-Time Approximate Equivalent Consumption Minimization Strategy Based on the Single-Shaft Parallel Hybrid Powertrain. *Energies* **2021**, *14*, 7919. <https://doi.org/10.3390/en14237919>

Academic Editor: Francesco Bottiglione

Received: 19 October 2021  
Accepted: 19 November 2021  
Published: 26 November 2021

**Publisher's Note:** MDPI stays neutral with regard to jurisdictional claims in published maps and institutional affiliations.



**Copyright:** © 2021 by the authors. Licensee MDPI, Basel, Switzerland. This article is an open access article distributed under the terms and conditions of the Creative Commons Attribution (CC BY) license (<https://creativecommons.org/licenses/by/4.0/>).

## 1. Introduction

In recent years, with the development of the automobile industry, the automobile has improved human life, but at the same time, it has also caused a significant increase in traffic energy consumption and the aggravation of urban haze. Achieving low energy consumption and low emissions has become the mainstream trend in the development of the automobile industry nowadays. Comprehensive existing industrial base, hybrid electric vehicle (HEV), and electric vehicle (EV) have become one of the best solutions to the problem at this stage [1,2]. The powertrain of HEV drives the vehicle through an electric motor to avoid the inefficient and polluting operation of the engine. The engine/motor hybrid mode optimizes output performance (e.g., acceleration and hill-climbing capability) for heavy-duty or high-power requirements [3,4]. For HEV architectures, the energy management strategy (EMS) is crucial. The main goal of the EMS is to meet the driver's traction requirements while maintaining the battery charge and optimizing driveline efficiency, fuel consumption, emissions, etc. More importantly, the real-time control of EMS is meaningful for HEV [5,6]. Therefore, how to develop a suitable EMS to achieve effective and fast power distribution for real-time control has been the theme and focus of attention.

At present, energy management control strategies can be divided into two different approaches: rule-based and optimization-based [7,8]. Rule-based control is characterized by fast rule design and easy implementation and has been widely used in real-time control

of hybrid vehicles. The operating modes of the vehicle are classified into three modes according to the vehicle speed, battery SOC, and demand power: electric mode, the engine drive mode, and the hybrid drive mode [9–11]. However, the set of rules usually relies on the experience of engineers, known mathematical models, a large amount of experimental data, etc. The method has very limited improvement in fuel-saving performance. For hybrid systems with nonlinear time-varying characteristics, fuzzy control is an effective way to solve its real-time energy management problem [12]. Denis et al. proposed a fuzzy-based EMS, proven to be effective, which focused on driving conditions for plug-in hybrid electric vehicles (PHEV) [13]. Since fuzzy controller does not require high accuracy in modeling and measurement of controlled targets, it can improve the robustness and adaptability of rule control. However, there is no mature law to follow when designing the affiliation function and fuzzy rules that play a decisive role in its control effect, and it can only rely on the designer's own knowledge and experience. Therefore, the optimization-based PMP and various intelligent methods for EMS are major areas of interest [14].

EMS based on optimization for vehicle simulation can be divided into two areas: global optimization and real-time optimization. Dynamic programming (DP) is widely applied in the EMS as a typical global optimization algorithm. The optimal control algorithm obtained from DP is the most representative energy management strategy based on optimal control theory. It transforms a multi-stage optimal decision problem into multiple single-stage optimal decision problems. Under the premise that the whole road working condition is known, the continuous state and control variables are discretized and the cost functions of all possible control sequences at each stage are calculated, and finally, the optimal solution is solved in reverse using the Bellman optimality principle [15]. In the literature [16,17], power distribution can be achieved using the DP approach for a fixed driving cycle. However, DP can only be optimized offline for a fixed driving cycle and the high computational cost of DP makes real-time control impossible [18,19].

For real-time applications, optimized fuel consumption needs to be performed quickly at each period. The equivalent consumption minimization strategy (ECMS) has received a lot of attention from researchers [20], which defines an equivalence factor to convert the equivalent fuel consumption from electricity consumption and power distribution which can be applied with at minimum the equivalent fuel consumption. ECMS was first proposed by Paganelli as a method for solving minima and was applied to hybrid powertrain energy management [21]. In Ref. [22], Geng, B., Mills, J.K., et al. proposed transient optimal energy management to minimize the equivalent fuel consumption. This strategy treats energy as an equivalent factor and battery power as a state variable, and updates the equivalent factor in real-time as the vehicle is driven. The equivalent factor is updated in real time as the vehicle is driven, and the output power of the motor and engine is corrected in real-time to achieve the goal of fuel-saving. Gao et al. applied ECMS to real-time to optimal control of PHEV and obtained better fuel economy and power retention performance [23]. In Refs. [24,25], the Approximate Pontryagin minimization principle (PMP) was applied to the suboptimal EMS. The real-time optimization strategy based on instantaneous equivalent fuel consumption minimization control can obtain the instantaneous optimal hybrid powertrain energy allocation for fuel economy and emissions in the current state of the vehicle. However, it needs to calculate the available power output combinations of the hybrid powertrain for each control step, which has a large computational load and high hardware real-time requirements.

Due to its fast convergence, low computational effort for a variety of applications such as system identification, network optimization, and power systems [26,27], the particle swarm algorithm (PSO) is suitable for real-time control. In Ref. [28], based on the CD strategy, the PSO is applied to the PHEV to optimize the control strategy parameters to maximize the fuel economy. Simulation results demonstrate that this method has a significant improvement in fuel economy without loss of vehicle performance. In Ref. [29], PSO was applied to real-time control of the vehicle to achieve online power distribution, and the improved particle swarm algorithm (IPSO) was used to improve the operation

speed of the algorithm with good results. In Ref. [30] Wang et al. applied a nonlinear model predictive control strategy based on particle swarm optimization to optimize fuel consumption in a series-parallel hybrid bus. In Ref. [31], Chen proposed that a dynamic particle swarm algorithm be applied based on ECMS for PHEV to realize torque distribution and gear output.

Although the PSO shows a great advantage in power distribution, the optimization-seeking iteration process still affects the computational load in real-time and the equivalence factor has an impact on fuel economy for ECMS [32]. Because of this, establishing fast and effective EMS is critical to improving fuel economy for real-time applications.

To reduce the computational load and improve fuel economy, this paper makes the following contribution. First, for the characteristics of the single-shaft parallel hybrid powertrain, Approximate-ECMS is proposed to reduce the computational load. The engine is fitted with a quadratic function for the fuel consumption rate and the fitness function is transformed into a cubic function by introducing a power assignment factor on the power distribution for solving based on ECMS. The second contribution concerns considering the equivalence factor, a hybrid DPSO-GA algorithm is presented for Approximate-ECMS to improve fuel economy. Finally, results showed that Approximate-ECMS have a great improvement in fuel economy compared with rule-ECMS and could reduce the computational load compare with PSO-ECMS. These findings prove Approximate-ECMS effectiveness.

## 2. Hybrid Powertrain System Configuration and Modeling

### 2.1. Hybrid Powertrain Configuration

In this paper, the parallel hybrid powertrain's structure is shown in Figure 1. The engine and the motor are installed on the same shaft, and the motor can be driven as a power source or recovered as a generator. The transmission system uses a six-speed AMT transmission to adjust the power source operating point. The clutch is located between the engine and the drive motor to realize the switching of multiple drive modes. Parallel hybrid electric vehicles have five typical operating modes: pure electric vehicle mode, engine drive mode, hybrid drive mode, regenerative braking mode, and drive charging mode. The objective of vehicle energy management is torque distribution. The torque distribution of the engine and motor is realized through mode switching to improve the fuel economy.

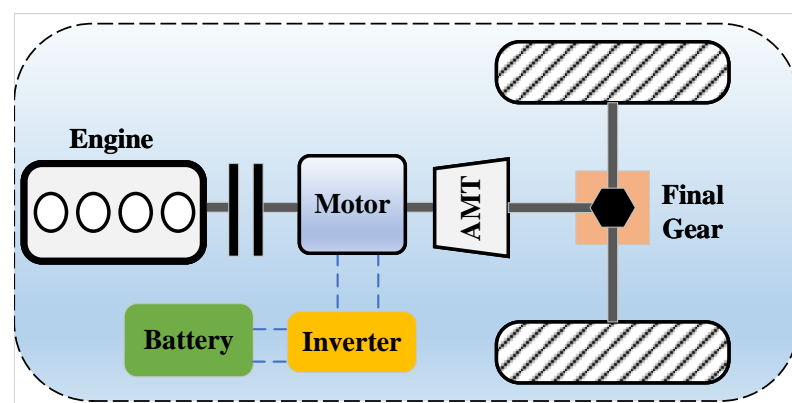


Figure 1. Hybrid powertrain structure.

### 2.2. System Modeling

#### 2.2.1. Engine Model

The engine model is built based on a spark gasoline engine. The energy management strategy (EMS) of a hybrid power system is related to engine fuel consumption  $Q_{fuel}$ .

Considering the complex dynamic characteristics of the engine, the fuel consumption model is simplified and written as:

$$Q_{fuel} = T_e \cdot \omega_e \cdot BSFC(t) \cdot \Delta t / 3600 = m_{fuel} \Delta t \quad (1)$$

where  $T_e$  and  $\omega_e$  are the engine torque and speed, respectively,  $m_{fuel}$  is the mass flow rate,  $BSFC(t)$  is the brake-specific fuel consumption (BSFC) of the engine, the BSFC uses a two-dimensional look-up table method and determines engine torque and speed in Figure 2.

$$BSFC(t) = function(T_e, \omega_e) \quad (2)$$

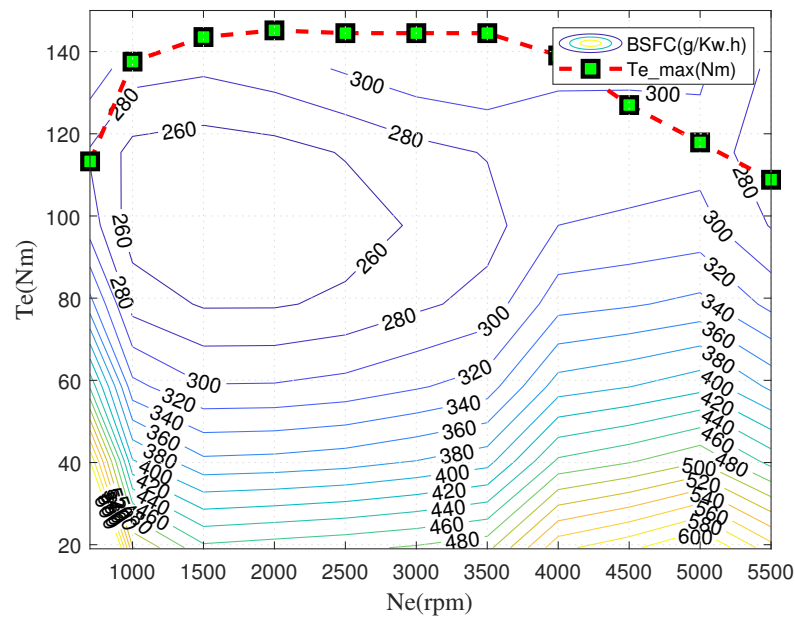


Figure 2. BSFC map of the engine.

### 2.2.2. Motor Model

To better adjust the engine operating point, a permanent magnet synchronous motor is used as a driving motor. It is selected as a motor for driving or as a generator for charging. The motor power can be written as

$$P_m = \begin{cases} T_m \cdot \omega_m / \eta_m, & (T_m > 0) \\ T_m \cdot \omega_m \cdot \eta_m, & (T_m < 0) \end{cases} \quad (3)$$

where  $T_m$  and  $\omega_m$  are the motor torque and speed, respectively. When  $T_m$  is positive, the motor works as a motor. On the contrary, when  $T_m$  is negative, the motor work as a generator.  $\eta_m$  is the motor efficiency in Figure 3, which is obtained according to the  $T_m$  and  $\omega_m$ .

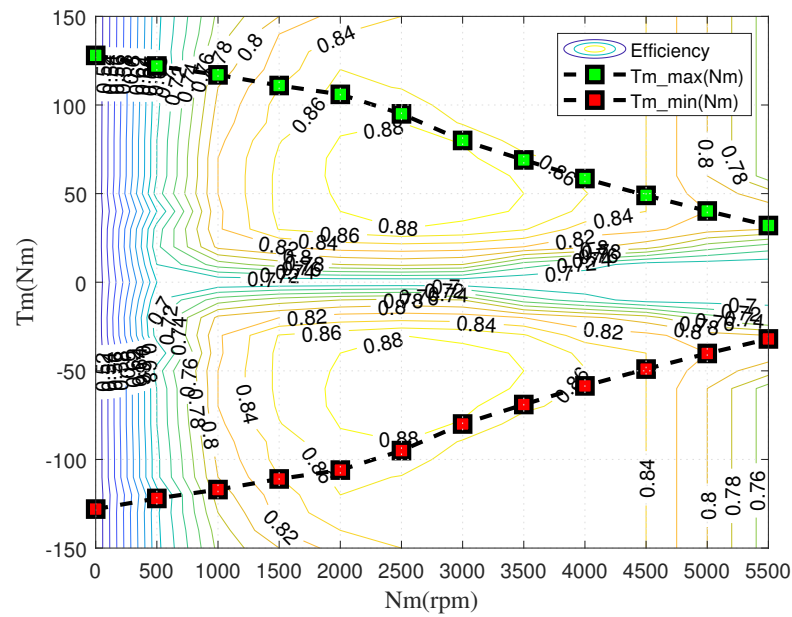


Figure 3. Efficiency map of the motor.

### 2.2.3. Battery Model

Battery charging and discharging are complex electrochemical reactions [33]. It is difficult to obtain accurate battery performance only through empirical formulas. The battery model can be built by combining experiments with empirical formulas, which is more accurate. Thus, the battery can be seen as an equivalent circuit of a voltage and a resistor as shown in Figure 4. According to the equivalent circuit of the battery internal resistance model [34], the voltage at battery terminals is written as

$$V_{batt} = E_{batt} - I_{batt}R_{batt} \quad (4)$$

where  $E_{batt}$ ,  $I_{batt}$  and  $R_{batt}$  are the open-circuit voltage, charge/discharge current, and internal resistance, respectively. Furthermore, the SOC rate of change and power can be described by the following equation:

$$\begin{cases} \dot{SOC} = -I_{batt}/Q_{batt} \\ P_{batt} = E_{batt}I_{batt} - I_{batt}^2R_{batt} \end{cases} \quad (5)$$

where  $P_{batt}$  and  $Q_{batt}$  are output power and the capacity of the battery, respectively. According to Equations (4) and (5), the SOC rate of change can be expressed by

$$\dot{SOC} = \frac{-E_{batt} + \sqrt{E_{batt}^2 - 4P_{batt}R_{batt}}}{2Q_{batt}R_{batt}} \quad (6)$$

where  $P_{batt} > 0$  represents discharging and  $P_{batt} < 0$  represents charging. To simplify the battery model, the temperature changes and battery aging are ignored. The open-circuit voltage and the internal resistance are related to the battery SOC, as shown in Figure 5.

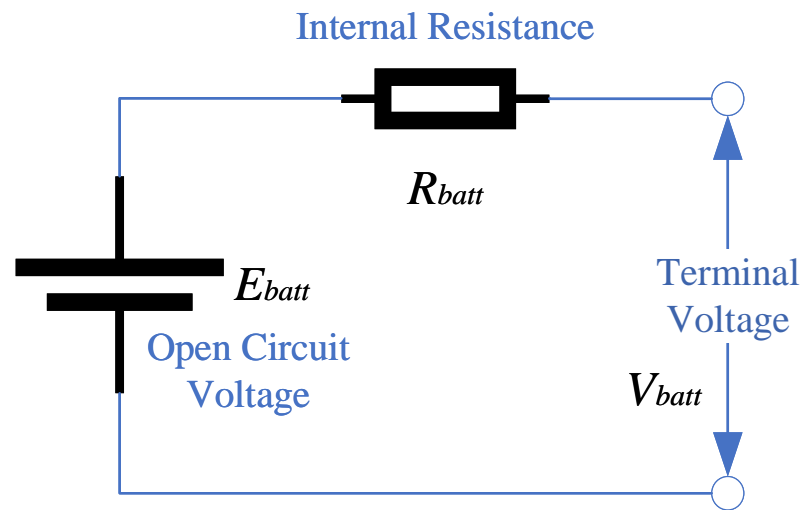


Figure 4. Rint model.

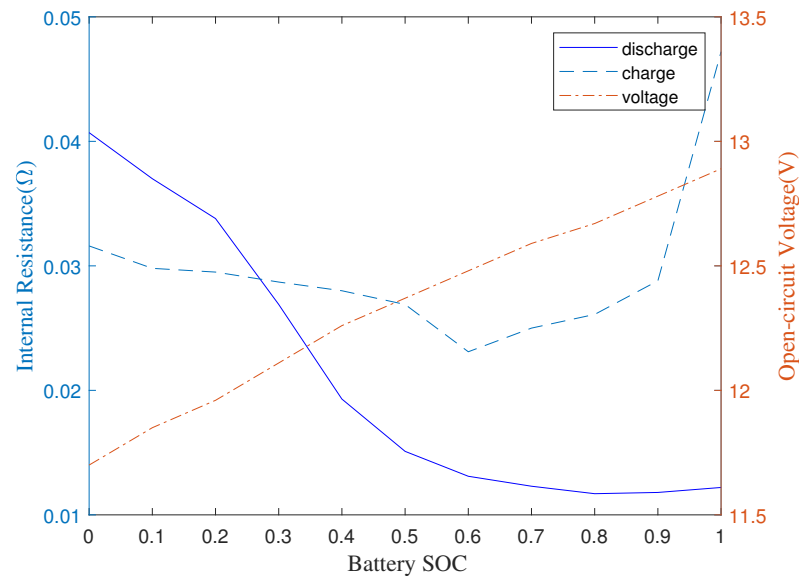


Figure 5. Internal resistance and open-circuit voltage.

### 2.2.4. Longitudinal Dynamics Model

The energy management strategy is related to the vehicle longitudinal dynamic model. Thus, lateral dynamics and steering dynamics are neglected. The relationship between  $T_w$  and the coupling torque of two power sources is shown as:

$$T_w = (T_e + T_m)i_{AMT}i_0\eta_T + T_{brake} \tag{7}$$

where  $T_w$  is output torque to drive,  $i_{AMT}$  and  $i_0$  are the reduction ratio of AMT and final gear ratio, respectively,  $\eta_T$  is the transmission efficiency.  $T_{brake}$  is the braking torque. According to the longitudinal dynamics of the vehicle, the  $T_w$  can be expressed as:

$$T_w = (mgf \sin \theta + mg \cos \theta + \frac{1}{2}C_D\rho Av^2 + \delta m \frac{dv}{dt}) \cdot R_w \tag{8}$$

where  $R_w$  is the wheel radius,  $m$   $g$   $C_D$   $\rho$  and  $A$  are the vehicle mass, gravity acceleration, air drag coefficient, air density, and frontal area, respectively,  $\theta$   $f$   $\delta$  and  $v$  represent road grade, rolling resistance coefficient, rotating mass coefficient, and vehicle velocity, respectively.

### 2.2.5. Driver Model

The driver model employs a proportional-integral (PI) controller. The speed error  $\Delta v$  between the reference speed  $v_d$  of the driving cycle and actual speed  $v_a$  is used as input to the controller. If  $\Delta v$  is positive, the controller outputs the required drive torque  $T_d$ , if negative, the controller outputs  $T_b$ , the required brake torque.

$$T_d = T_{hy} [k_p (v_d(t) - v_a(t)) + k_I \int_0^t (v_d(t) - v_a(t)) dt] \quad v_d(t) - v_a(t) > 0 \quad (9)$$

$$T_b = T_{brk} [k_p (v_d(t) - v_a(t)) + k_I \int_0^t (v_d(t) - v_a(t)) dt] \quad v_d(t) - v_a(t) < 0 \quad (10)$$

where  $T_{hy}$  and  $T_{brk}$  are the maximum drive torque and maximum braking torque, respectively;  $k_p$  and  $k_I$  represent proportional gain value and integral gain value, respectively.

## 3. Energy Management Control Strategies

### 3.1. Energy Management-Based Ruled

Rule-based energy management strategy (Rule-EMS) is more dependent on engineering experience and work patterns and is not influenced by precise minimization or optimization. Most rule-based control policies control the system in an “if-else” fashion and maintain load balancing within the system. According to the literature [29], the rule-based policy design consists of six patterns, as shown in Table 1.

**Table 1.** Operating modes and rule-based control.

Operation Mode	Conditions	Torque Distribution
1. Stop mode	$N_e = 0 \&\& T_d = 0$	$T_e = 0, T_m = 0$
2. Motor-only mode	$0 < N_e < 1800$	$T_e = 0, T_m = T_d$
3. Engine-only mode	$1800 < N_e < 2300$	$T_e = T_d, T_m = 0$
4. Hybrid mode	$N_e > 2300$	$T_e = 0.7 * T_d, T_m = 0.3 * T_d$
5. Recharging mode	$0.3 < SOC < 0.5$	$T_e = T_d + 20, T_m = -20$
6. Regenerative braking mode	$T_d < 0 \&\& SOC < SOC_{up}$	$If T_d < T_{m\_max}, T_d = T_m$ $If T_d > T_{m\_max},$ $T_d = T_{m\_max} + T_{mechanic}$

### 3.2. Approximate-ECMS Strategy

#### 3.2.1. Power Allocation Factor

The power allocation factor is introduced as a control variable for energy management, which plays a role to adjust the engine’s best working line dynamically to get a better fuel economy. It is defined as follows:

$$k_{p\_split} = P_e / P_d = T_e * N_e / T_d * N_d \quad (11)$$

As it is a single-axis tandem structure and the two power sources are located in front of the gearbox, the engine speed is the same as the motor speed.

$$N_d = N_e = N_m \quad (12)$$

The motor torque and engine torque can be written as

$$T_e = k_{p\_split} * T_d, T_m = (1 - k_{p\_split}) * T_d \quad (13)$$

#### 3.2.2. Basic of ECMS

The central idea of a real-time optimization algorithm is to calculate the fuel consumption and power consumption corresponding to all combinations of engine and motor output torques that meet the driver’s demand torque at each moment of the vehicle driving process. The instantaneous fuel consumption is expressed as the equivalent fuel consump-

tion of engine fuel consumption and power consumption. Additionally, the motor output torque is adjusted to obtain the minimum value of this instantaneous fuel consumption. Finally, the combination of engine and motor output torque corresponding to this minimum value is used as the working point [35]. Therefore, equivalent fuel consumption can be expressed as in the following equation:

$$J(x, u) = \int_{t_0}^{t_f} \dot{m}_{eq} dt = \int_{t_0}^{t_f} [\dot{m}_{fuel}(x, u) + \dot{m}_{batt}(x, u)] dt \quad (14)$$

$$\dot{x} = f(x, u) \quad (15)$$

$$\begin{cases} x_{\min} \leq x \leq x_{\max} \\ u_{\min} \leq u \leq u_{\max} \end{cases} \quad (16)$$

where  $\dot{m}_{batt}$  represents the battery fuel consumption rate,  $x$  and  $u$  are the state and control variables, respectively.  $t_0$  and  $t_f$  are the initial time and final time.

$$\begin{cases} x = SOC \\ u = T_m \end{cases} \quad (17)$$

For the above optimal control strategy objective function, the constrained problem is transformed into an unconstrained problem solved using the principle of minimal values. According to Pontryagin's Minimum Principle (PMP), the Hamiltonian can be expressed by the following equation.

$$H(x, u, \lambda, t) = \dot{m}_f(u, t) + \lambda t * \dot{SOC}(t) \quad (18)$$

where  $\lambda(t)$  indicates the co-state. In a hybrid powertrain, the electric motor and engine are mixed to meet the driver's demand torque, so the amount of fuel consumed by the car has a direct effect on the battery power  $P_B$ . At a certain demand power, the increase of battery power has a decrease in fuel consumption. Further, the Hamiltonian can be rewritten as

$$H(x, u, \lambda, t) = \dot{m}_f(P_B) + \lambda(t) \cdot f(x, P_B) \quad (19)$$

The regular Hamiltonian equation is as follows:

$$\dot{x} = \frac{\partial H}{\partial \lambda} = f(x, P_B) \quad (20)$$

$$\dot{\lambda}(t) = -\frac{\partial H}{\partial x} = -\lambda(t) \frac{\partial f}{\partial x} = -\frac{\partial H(SOC(t), P_B, \lambda(t))}{\partial SOC} \quad (21)$$

From Figure 5 the open-circuit voltage and internal resistance of the battery pack are constant values, which are not related to SOC. According to the principle of minimal values, the optimal co-state is obtained by

$$\dot{\lambda}^*(t) = -\dot{\lambda}^*(t) \frac{\partial f}{\partial x} = 0 \quad (22)$$

Therefore,  $\lambda^*(t)$  is constant. It is shown that a globally optimal solution can be generated when the co-state  $\lambda^*(t)$  is a constant.

$$H(x^*, \lambda^*, u^*, t) = \min H(x^*, \lambda^*, u^*, t) \quad (23)$$

where the superscript \* indicates the optimal. Then the Hamiltonian function can be transformed into a cost function, which is further written as

$$H = \dot{m}_f + \frac{S(t)}{Q_{lhv}} P_B \quad (24)$$

where  $S(t)$  is defined as the equivalent factor (EF),

$$S(t) = \begin{cases} S_{chg} = \frac{\bar{\eta}_{m\_drive} \bar{\eta}_{B\_dis}}{\bar{\eta}_e} & P_B > 0 \\ S_{dis} = \bar{\eta}_{m\_gen} \bar{\eta}_{B\_chg} \bar{\eta}_e & P_B < 0 \end{cases} \quad (25)$$

$$P_B = \begin{cases} P_m \eta_{m\_drive} \eta_{B\_chg} & \text{charging} \\ \frac{P_m}{\eta_{m\_drive} \eta_{B\_dis}} & \text{discharging} \end{cases} \quad (26)$$

where  $P_m$  is the motor power,  $S_{chg}$  and  $S_{dis}$  are EFs in the driving and generating mode, respectively,  $\eta_{m\_drive}$  and  $\eta_{m\_gen}$  are the working efficiency of the electric motor in driving and generating mode, respectively,  $\bar{\eta}_{m\_drive}$  and  $\bar{\eta}_{m\_gen}$  are the working average efficiency of the electric motor in driving and generating mode, respectively,  $\bar{\eta}_{B\_dis}$  and  $\bar{\eta}_{B\_chg}$  represent the battery charging and discharging average efficiency,  $\bar{\eta}_e$  is the average working efficiency of the engine,  $Q_{lhv}$  is the fuel low calorific value. From Equation (24), the equivalent factor has a direct effect on torque distribution between engine and motor.

### 3.2.3. Approximate-ECMS

The control strategy based on the minimal value principle transforms global optimization into instantaneous optimization, so theoretically the control strategy can be applied to real-time control. However, the Hamiltonian function is a complex function of the control variable  $u(t)$  and the search for the optimal control needs to be spread over the entire control variable domain. The control strategy based on the principle of minimal values requires a large amount of computation and time, which makes it difficult to realize real-time control in practice. Therefore, an approximate minimum value principle real-time control strategy is proposed to reduce the search time by simplifying the optimal control variable search space based on fitting the instantaneous engine fuel consumption. Unlike previous studies, the Approximate-ECMS is innovatively applied in this study based on the characteristic of the vehicle's single-axis parallel-type structure. The engine fuel consumption rate curve is shown in Figure 6. The engine fuel consumption rate ( $b_e$ ) curve is represented by a quadratic function fit and curve with torque at a determined speed.

$$b_e = aT_e^2 + bT_e + c \quad (27)$$

$$\dot{m}_{fuel} = b_e * P_e / 1000 / 3600 \quad (28)$$

where  $a$ ,  $b$ , and  $c$  are the quadratic function fitting coefficients. By introducing the power allocation factor  $k_{p\_split}$ , the mass flow rate can be expressed as

$$\dot{m}_{fuel} = [a(k_{p\_split} * T_d)^2 + b(k_{p\_split} * T_d) + c] * (k_{p\_split} * T_d) * N_e / 9550 / 1000 / 3600 \quad (29)$$

$$\begin{cases} \dot{m}_{batt} = (\frac{S_{dis}}{Q_{lhv}} * P_m * \frac{1}{\eta_{m\_drive} \eta_{B\_chg}}) / 9550 / 1000 / 3600; SOC > SOC_{tar} \\ \dot{m}_{batt} = (\frac{S_{chg}}{Q_{lhv}} * P_m * \eta_{m\_drive} \eta_{B\_chg}) / 9550 / 1000 / 3600; SOC < SOC_{tar} \end{cases} \quad (30)$$

When  $S(t) = S_{opt}$ , the motor efficiency and battery efficiency are set to be fixed.

$$\begin{cases} p = \frac{S_{opt}}{Q_{lhv}} * \frac{1}{\eta_{m\_drive} \eta_{B\_dis}} & SOC > SOC_{tar} \\ p = \frac{S_{opt}}{Q_{lhv}} * \eta_{m\_drive} \eta_{B\_chg} & SOC < SOC_{tar} \end{cases} \quad (31)$$

The  $p$  has a constant value. The equivalent fuel consumption for the electric power from the battery  $\dot{m}_{batt}$  can be written as

$$\begin{cases} \dot{m}_{batt} = p * T_m * N_m / 9550 / 1000 / 3600 \\ \dot{m}_{batt} = p * 1 - k_{p\_split} * T_d * N_m / 9550 / 1000 / 3600 \end{cases} \quad (32)$$

At a certain point in the driving cycle, the speed and required torque are given. Thus, the equivalent fuel consumption equation can be transformed into a cubic function on the power distribution. According to the fitted curve of engine fuel consumption rate ( $b_e$ ) in Figure 6, it can be seen that the curve is an open-up quadratic function. Therefore,  $a > 0$ , further  $A > 0$ . Based on the graph and properties of the cubic function, when the discriminant  $\Delta > 0$ , the function has extreme values in the case of  $A > 0$ . The extreme value points are  $x_1$  and  $x_2$ , respectively. When the discriminant  $\Delta < 0$ , the function does not have extreme values and is a monotonic increasing function. The above mentioned can be referred to the Figures 7 and 8.

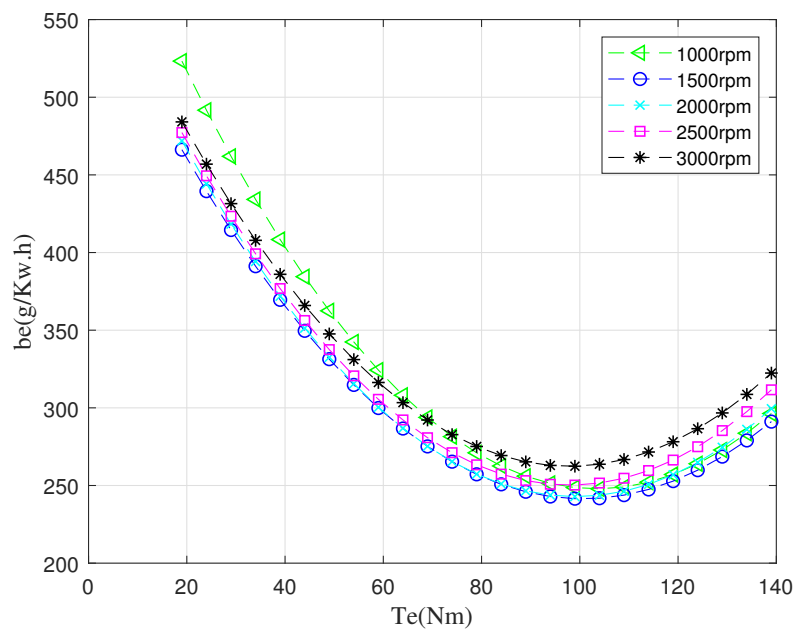


Figure 6. The engine fuel consumption rate ( $b_e$ ) curve.

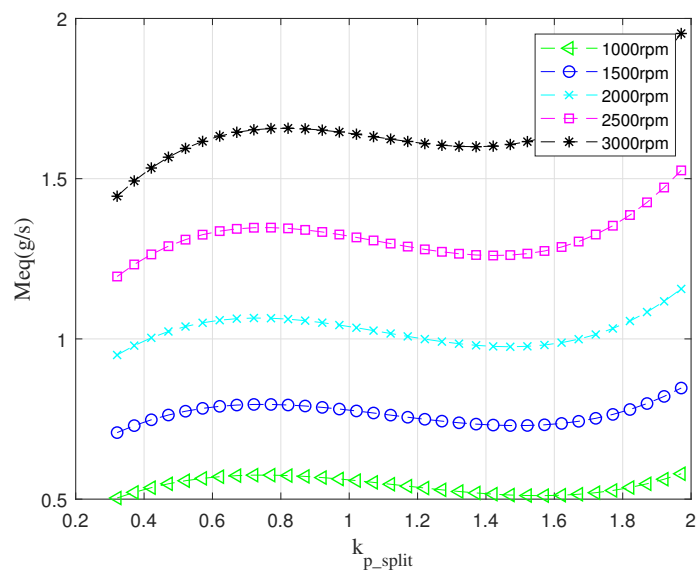


Figure 7. The equivalent fuel consumption (Meq) rate when  $T_d = 60N.m$ ,  $SOC = 0.65$ .

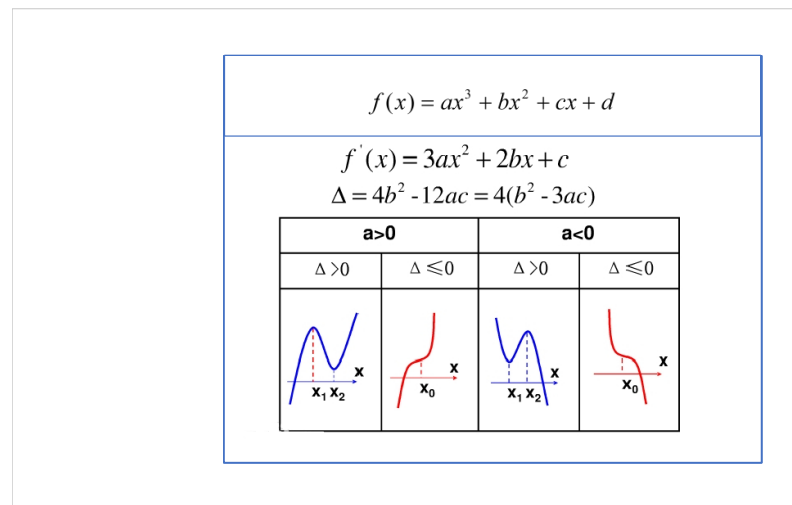


Figure 8. The image and properties of cubic function.

$$\dot{m}_{equ} = \dot{m}_{fuel} + \dot{m}_{batt} \quad (33)$$

We replace the cubic function on  $k_{p\_split}$  with  $f(k_{p\_split})$  for further rewriting

$$\dot{m}_{equ}(k_{p\_split}) = f(k_{p\_split})N_d/9550/1000/3600 \quad (34)$$

$$A = a * T_d^2, B = b * T_d, C = c - p, D = p \quad (35)$$

where  $A, B, C,$  and  $D$  are the  $f(k_{p\_split})$ 's coefficients.

$$f(k_{p\_split}) = A * k_{p\_split}^3 + B * k_{p\_split}^2 + C * k_{p\_split} + D \quad (36)$$

The derivation of the above equation gives:

$$f'(k_{p\_split}) = 3Ak_{p\_split}^2 + 2Bk_{p\_split} + C \quad (37)$$

$$\Delta = (2B)^2 - 4 * (3A)C \quad (38)$$

When  $\Delta > 0$ ,  $x_1$  is the maximum value,  $x_2$  is the minimum value.

$$\begin{cases} x_1 = (-2B - \sqrt{((2B)^2 - 4(2A)C)}) / (2 * 3A) \\ x_2 = (-2B + \sqrt{((2B)^2 - 4(2A)C)}) / (2 * 3A) \end{cases} \quad (39)$$

According to Equation (10),  $k_{p\_split}$  is the ratio of engine torque to demand torque. Since both the engine and motor have limits,  $k_{p\_split}$  are also limited. When  $SOC > SOC_{tar}$ , the range  $k_{p\_split}$  is as in Equation (40). When  $\Delta > 0$ , four candidates  $(1 - T_{m\_max}/T_d, 1, x_1, x_2)$  or  $(T_{e\_min}/T_d, 1, x_1, x_2)$  are calculated by Equation (33) and are chosen minimum as the optimal control for each time step.

### 3.2.4. Flow Diagram of the Approximate-ECMS

The flow chart of the Approximate-ECMS optimization process is shown in Figure 9. This strategy includes three steps. The first step is to derive the current fitting coefficients from the fitting database based on the current demand torque and speed. In the second step, the electrical power is transformed into equivalent fuel consumption by applying the equivalent factor. Thus a functional model on power distribution factor is developed. By calculating the discriminant, it is determined whether it is greater than zero. We compare the equivalent fuel consumption under the candidate solution and obtain the optimal power allocation factor corresponding to the optional Hamiltonian quantity. The optimal

power allocation factor is translated into the respective engine torque and motor torque. The engine torque command and motor torque command are sent to the power source.

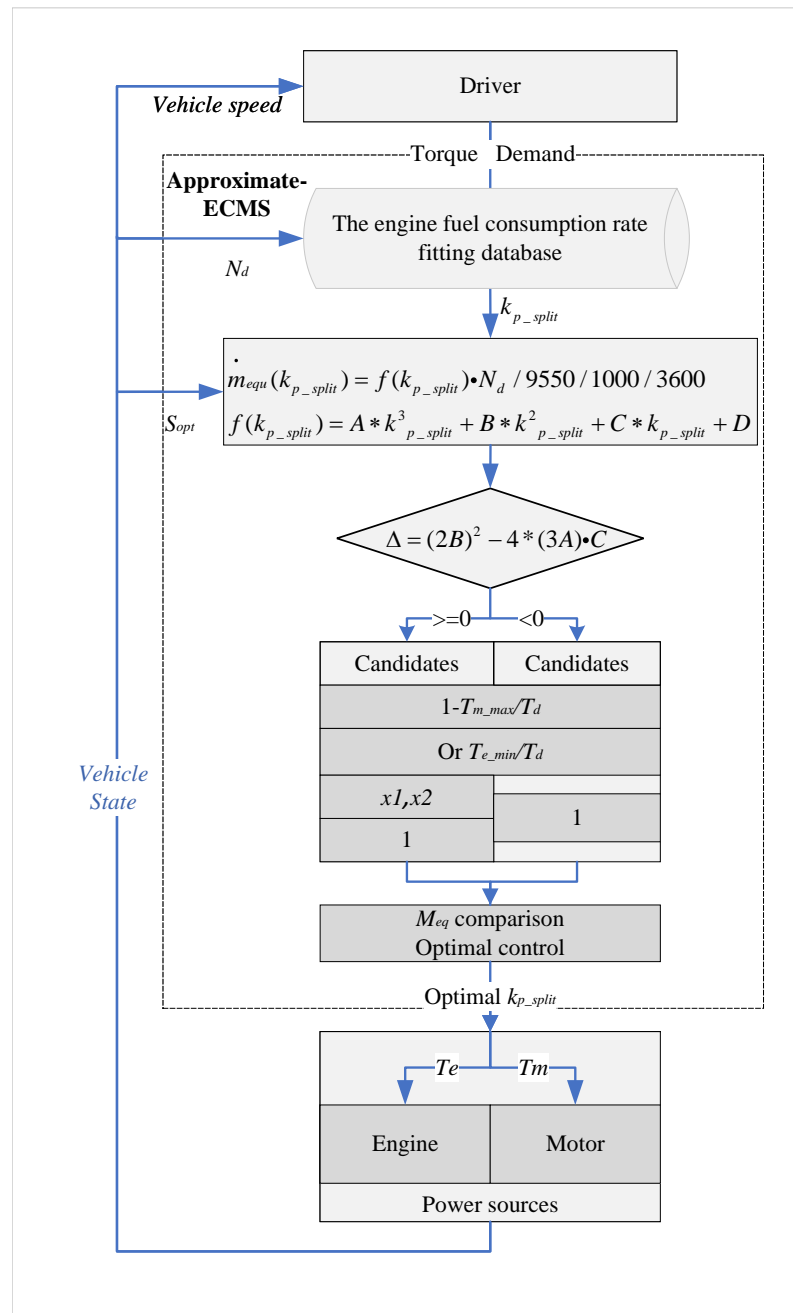


Figure 9. Flow diagram of the Approximate-ECMS.

#### 4. Equivalent Factor Optimization Based on DPSO-GA

The equivalence factor is a crucial parameter of the ECMS strategy and its magnitude determines the distribution of vehicle drive power between the engine and battery. The objective function of ECMS is to minimize the total equivalent fuel consumption of the system, but if only the total equivalent fuel consumption is considered, it will inevitably lead to the difficulty of maintaining the battery power balance. From the perspective of maintaining the battery power balance, the difference between the SOC termination value and the target value should be minimized [36,37]. Therefore, the optimization of ECMS is a multi-objective optimization problem, which requires to keep the total equivalent fuel consumption and the difference between the SOC termination value and target value at the

same time. The Approximate-ECMS calculation process shows that the main variables in the calculation of total equivalent fuel consumption are the equivalence factor and power allocation factor.

According to the literature [31], to achieve the global SOC variation law, the SOC penalty factor is introduced to realize the optimal power assignment based on the difference between the actual SOC and the target SOC. The SOC linear penalty function is expressed as follows:

$$\delta(\text{SOC}) = 1 - \beta \times \left( \frac{\text{SOC}(t) - \text{SOC}_{tar}}{\text{SOC}(t) - \text{SOC}_{low}} \right) \times 2 \quad (40)$$

where  $\beta$  denotes a coefficient which is selected according to experience,  $\beta = 0.2$ ,  $\delta(\text{SOC})$  is the SOC penalty factor,  $\text{SOC}(t)$  is the battery SOC at time  $t$ ,  $\text{SOC}_{low}$  and  $\text{SOC}_{tar}$  are low SOC and the target SOC of battery, respectively. The relationship between the penalty value, and  $\text{SOC}(t)$  of the battery is shown in Figure 10. With the increase of the SOC, the penalty factor value decreased, when  $\beta$  was fixed.

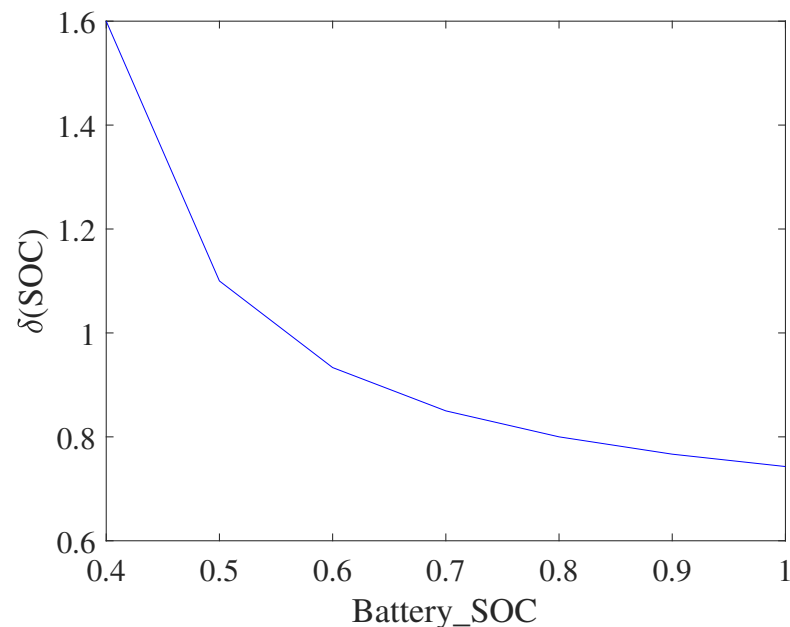


**Figure 10.** The SOC linear penalty function.

The equivalence factor can be expressed as Equation (42). From the equation, it is clear that the initial value of the equivalent factor affects the overall change of the equivalence factor. Therefore, it is necessary to optimize the initial value of the equivalent factor.

$$S_{opt} = \delta(\text{SOC})s_0 \quad (41)$$

where  $s_0$  is the initial value of the equivalent factor

#### 4.1. Hybrid DPSO-GA-Based Optimization Algorithm

Among optimization algorithms, particle swarm algorithm and genetic algorithm are commonly used population-based algorithms, but they both have advantages and disadvantages [38,39]. The particle swarm optimization algorithm is simple to operate and fast to compute, but the particles with low adaptation values are slow to update and contribute little to the particle population. While genetic algorithms are relatively complex, crossover and mutation operations lead to individual variation. In other words, an individual with poor fitness may become a more adaptive individual through crossover and mutation. Hybrid algorithms based on particle swarm-genetic algorithms combine particle swarm algorithms and genetic algorithms to maintain the advantages of both. In

this section, the dynamic particle swarm algorithm optimization and genetic algorithm strategy are applied to optimize the equivalent factor.

#### 4.1.1. Basic Principle of Dynamic Particle Swarm Optimization

PSO is a simulation of the predatory behavior of a flock of birds searching for food randomly. There is an exchange of information between birds. The distance between the current position and the food is determined by estimating its fitness value. Searching the area of the bird currently closest to food is the easiest and most efficient way to find food. PSO is inspired by this model and used to solve optimization problems. The PSO algorithm is a type of evolutionary algorithm, which starts from a set of random solutions and iterates to find the optimal solution. In each iteration, the particle updates itself by two extremes. The first one is the optimal solution of the particle itself and the other one is the current optimal solution of the whole population [31]. In finding the two optimal values, the particle updates its velocity and position according to the following Equations (42) and (43).

$$\begin{aligned} v_{id}^{t+1} &= \omega * v_{id}^t + c_1 r_1 (p_{id} - x_{id}^t) + c_2 r_2 (p_{gd} - x_{id}^t) \\ x_{id}^{t+1} &= x_{id}^t + v_{id}^t \end{aligned} \quad (42)$$

where  $\omega$  is the inertia weight;  $t$  is the number of current iterations;  $d$  is the particle dimension, and  $x_{id}^t$  are the velocity and position of the  $i$ -th particle in the  $d$ -th dimension at time  $t$ ;  $c_1$  and  $c_2$  are the learning factors;  $r_1$  and  $r_2$  are random numbers within  $[0,1]$ ;  $p_{id}$  is the best position of the  $i$ -th particle in the  $d$ -th dimension;  $g_{id}$  is the best position of all particles.

In the PSO, the inertia weight  $\omega$  is the most important parameter. Increasing the value  $\omega$  can improve the global search ability of the algorithm, and decreasing the value  $\omega$  can improve the local search ability of the algorithm. Therefore, designing reasonable inertia weight is the key to avoid falling into local optimum and search efficiently. In this paper, the dynamic inertia weight is adopted to improve the PSO performance. The dynamic inertia weight is determined by the following equation.

$$\omega = \begin{cases} \omega_{\min} - \frac{(\omega_{\max} - \omega_{\min}) * (f_i - f_{\min})}{f_{avg} - f_{\min}} & f_i \leq f_{avg} \\ \omega_{\max} & f_i > f_{avg} \end{cases} \quad (43)$$

where  $\omega_{\max}$  and  $\omega_{\min}$  are the maximum and minimum inertia weights, respectively.  $f_i$  is the fitness value of  $i$ -th particle.  $f_{avg}$  and  $f_{\min}$  denote the average and minimum fitness values of all current particles, respectively. The above equations show that the inertia weight changes with the change of particle fitness value. When the particle fitness values are scattered, the inertia weight is reduced; when the particle fitness values are consistent, the inertia weight is increased.

#### 4.1.2. Procedures of DPSO-GA

In the hybrid particle swarm algorithm, the dynamic particle swarm algorithm is used as the main body, and the cross-variance operation is introduced in the particle update. When performing a particle update, the adaptation degree of the particles is first determined. The particles with higher fitness values are updated by the particle swarm algorithm, and the velocity of each particle, also called potential solution, changes toward the global optimum (g-best) and the optimum of its personnel (p-best) of contemporary particles. In general, each particle adjusts its position based on its experience and that of its neighbors, including the current velocity, position, and the most favorable previous position. Conversely, particles with lower adaptation values are updated by crossover and mutation based on genetic algorithms [40]. The process of the hybrid particle swarm algorithm is shown in Figure 11.

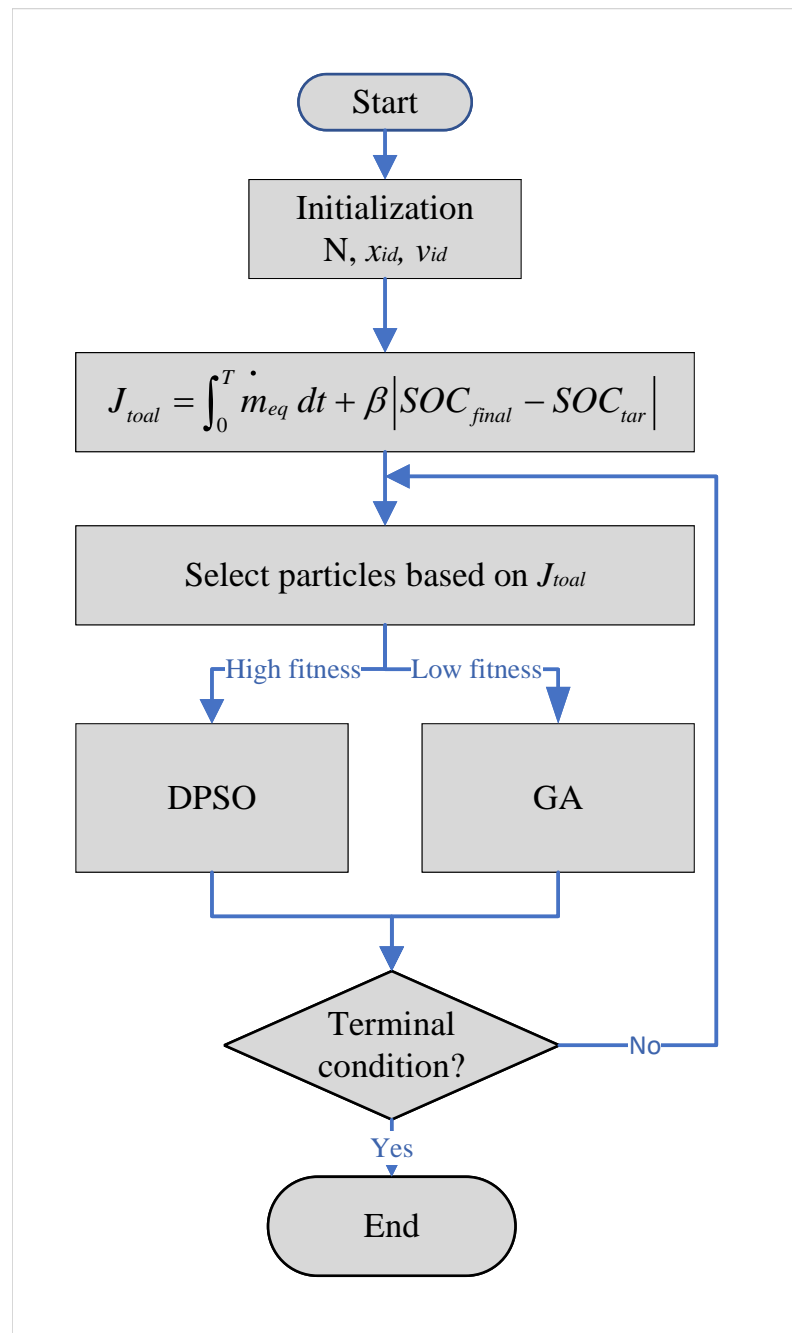


**Figure 11.** The process of the hybrid particle swarm algorithm.

1. Initialize particle swarm including swarm number  $N$ , particle position  $x_{id}$ , and velocity  $v_{id}$ . Initialize  $x_{id}$  and  $v_{id}$  of the particles, which are the initial value of the equivalent factor  $s_0$  and its variation, respectively.
2. The objective function: The goal of optimization is to achieve equivalent fuel consumption under typical driving cycles and to keep the difference between the final value of and the target value of SOC to a minimum, as shown in Equation (44).

$$J_{total} = \int_0^T \dot{m}_{eq} dt + \beta |SOC_{final} - SOC_{tar}| \quad (44)$$

where  $J_{total}$  is the objective function;  $\dot{m}_{eq}$  is the instantaneous fuel consumption obtained from Equation (13);  $T$  is the end time of driving cycles, and  $SOC_{tar}$  are the final and target value of SOC, respectively;  $\beta$  is the weighting factor.

3. Select particles based on ranked fitness and update: After initializing the particle swarm, the particle fitness is ranked according to the objective function. The function with high fitness is selected for particle swarm algorithm update based on Equation (43) and for low fitness values a genetic algorithm update is performed.
4. End: Set the termination condition. If the termination condition is not satisfied, execute steps 2–3 until the particle search satisfies the termination condition. Then obtain the best solution.

## 5. Simulation Results and Discussion

In this study, four different EMS were simulated for a hybrid powertrain system, including Rule-EMS, Basic-ECMS, PSO-ECMS, and Approximate-ECMS. These results are presented in this section and they are analyzed and compared, further illustrating the effectiveness of the proposed Approximate-ECMS strategy. To further obtain a good fuel-saving strategy, the results of the optimized equivalence factors were compared, thus demonstrating the effect of the initial equivalence factors on fuel saving.

### 5.1. Model and Settings of the Vehicle

The model of the vehicle was built on the MATLAB/Simulink platform. The sampling time was set to a fixed sampling time of 0.01 s and the Bogacki–Shampine solver was selected. Approximate-ECMS is programmed as an S function block in the torque splitting layer of the VCU. The parameters of the vehicle are listed in Table 2.

**Table 2.** The parameters of the vehicle.

Component	Parameters	Value
Engine	Engine type	1.9L.SI
	Maximum Power	63 kW @ 5500 rpm.
	Peak Torque	145 Nm @ 2000 rpm.
Motor	Motor type	Permanent magnet motor
	Maximum power	25 kW
Battery	Battery type	Lithium–ion
	Capacity	25 Ah
Vehicle	Vehicle mass	1350 kg
	Radius of tire	0.282 m
	Vehicle front area	2 m <sup>2</sup>
	Rolling resistance coefficient	0.014
	Aerodynamic drag coefficient	0.335

### 5.2. Comparison of Rule-EMS, Basic-ECMS, PSO-ECMS, and Approximate-ECMS

Figures 12–14 shows the simulation results during the NEDC driving cycle. The simulation results at  $SOC_{init} = 0.7$ . As shown in the first row of Figure 12, the actual velocity ( $V_a$ ) tracks the demand velocity ( $V_d$ ) very well for the test NEDC driving cycle. As shown in the first row of Figure 12, the actual velocity ( $V_a$ ) tracks the demand velocity ( $V_d$ ) very well for the test NEDC driving cycle due to the proper selection of the PI control parameters for the drive model in Equations (10) and (11). The speed tracking is very good (within  $\pm 0.5$  km/h), which means that the following simulation results based on four EMS are plausible. In the second row, power allocation factor ( $k_{p\_split}$ ) results for Rule-EMS control based on Table 1 are presented. It can be seen that during acceleration the motor drive alone works at low-speed demand and the engine alone works at medium speed. Combined motor and engine drive working at high speed. The third row shows the Basic-ECMS online simulation results according to the PMP in Equation (23). Allocation of the optimal engine and motor torque at moderate speed and high speed by minimizing equivalent fuel consumption. The fourth row is the online assignment of the PSO-ECMS

proposed in the literature [23]. The fifth row is the Approximate-ECMS mentioned along with this paper. The simulation results of Approximate-ECMS are very similar to PSO-ECMS. However, PSO-ECMS uses more electric power at high speeds. The motor works alone when the speed is less than the engine's minimum speed with sufficient power. Since the method of quadratic root-finding used by Approximate-ECMS is within the constraint, the simulation is faster than PSO-ECMS.

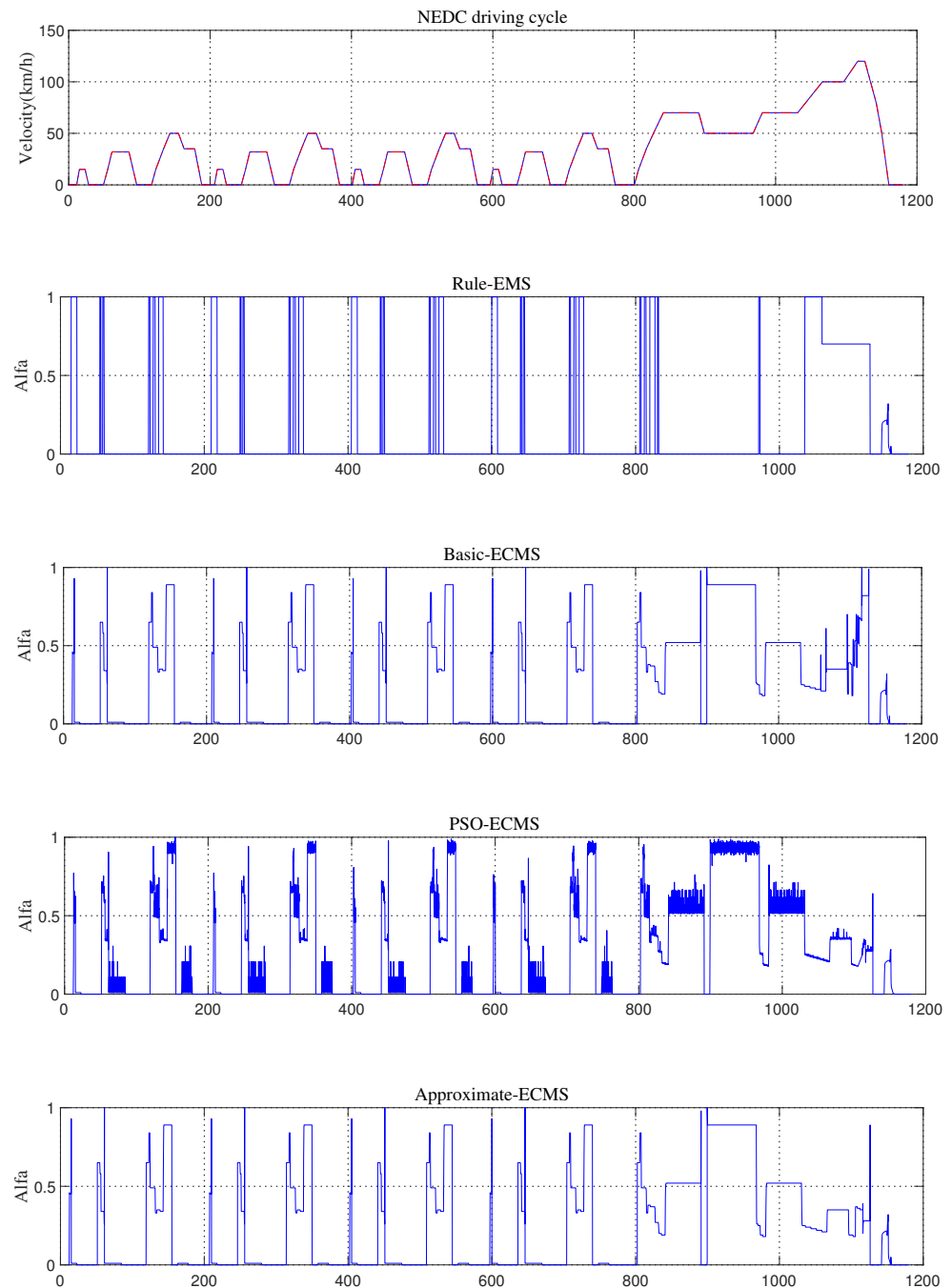


**Figure 12.** Speed profiles, Rule-EMS, Basic-ECMS, PSO-ECMS, and Approximate-ECMS at  $SOC_{init} = 0.7$ .

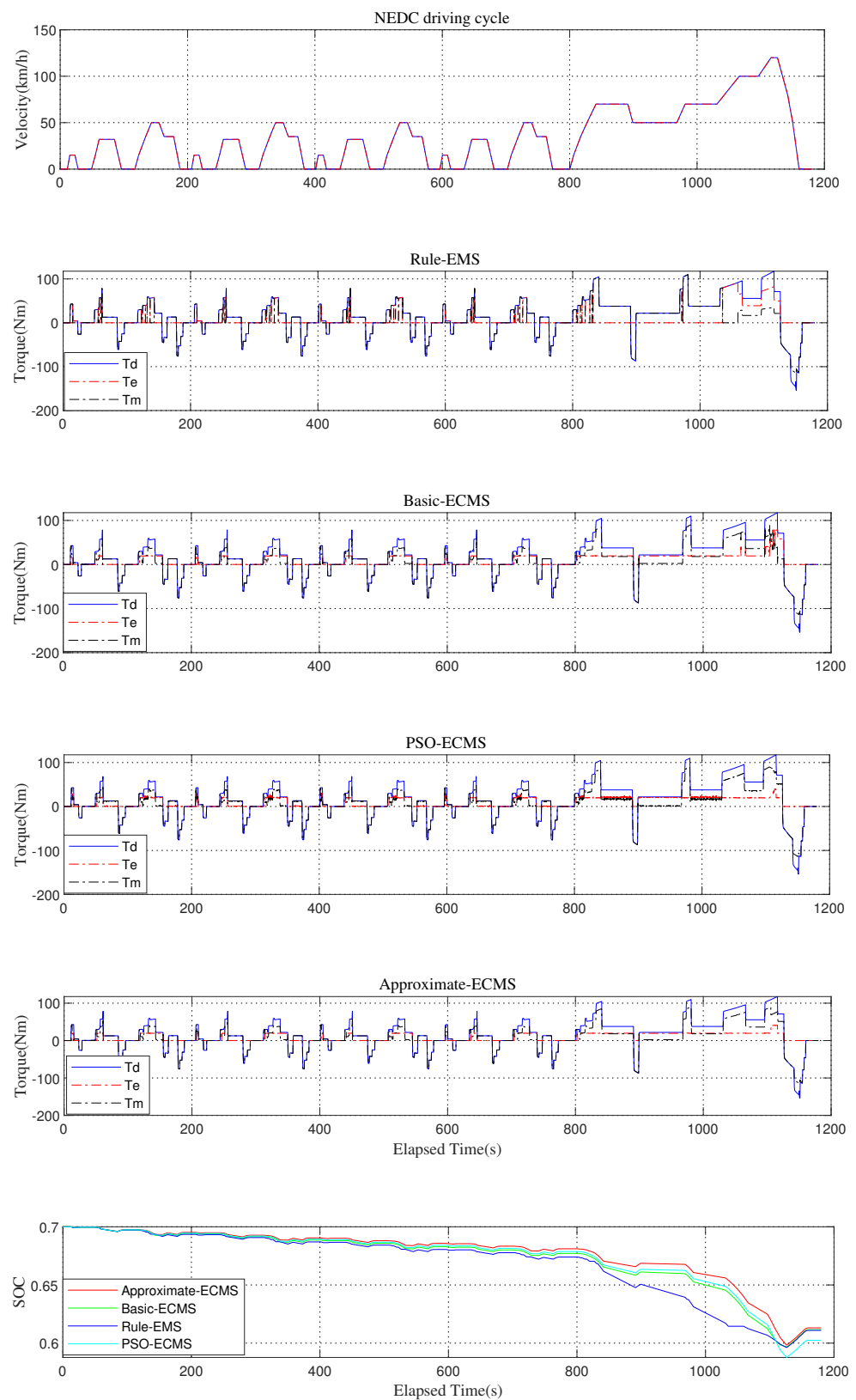


**Figure 13.** /hlSpeed profiles, Torque of Rule-EMS, Basic-ECMS, PSO-ECMS, and Approximate-ECMS at  $SOC_{init} = 0.7$ .

In order to illustrate the different aspects of these four EMS, the torque results for the four cases are shown in Figure 13. For the Rule-EMS control in the first row, the demand torque is distributed to the engine and motor according to the demand speed.

The motor provides torque at low speed. At medium speed the engine offers torque. Engine and motor together provide torque at high speed. As for Basic-ECMS, PSO-ECMS, and Approximate-ECMS, the torque distribution is based on the power allocation factor  $k_{p\_split}$ . From the second to the fourth row above it can be seen that demanded torque distribution is approximately the same at low velocity. When the demand speed is less than the minimum engine speed or the motor is in recovery mode, the demand torque motor is provided alone. Thus, during deceleration,  $k_{p\_split}$  is zero. During acceleration, as  $k_{p\_split}$  increases, it indicates that the engine is providing more power to save electricity. The fifth row shows the SOC change trajectory of four cases. As can be seen, in the low and medium speed region, the motor consumption is lower due to the active engine involvement with Basic-ECMS, PSO-ECMS, and Approximate-ECMS control. Therefore, in the Rule-EMS control, SOC decreases faster. After 1000 s, due to active motor assistance, the SOC of Basic-ECMS, PSO-ECMS, and Approximate-ECMS control decrease faster than Rule-EMS control.

Figure 14 illustrates the efficient operation of the engine during four EMS control processes. In the Rule-EMS control process, the engine mostly operates in a low-efficiency region, where the BSFC is mostly within 340–450 g/kW.h. With Basic-ECMS, PSO-ECMS, and Approximate-ECMS control, the engine mostly runs in a more efficient region where the BSFC is within approximately 280–400 g/kW.h and the small part of the engine works at the BSFC 240–280 g/kW h. The operating points of the motor are located in the effective region (between 75% and 85% efficiency) in the rule-based control case. The distribution of the operating points in the PSO-ECMS and Approximate-ECMS cases is similar. Most of these points are located in the effective region, where the operating points are concentrated around 88%. The engine operating point of the Approximate-ECMS control as a whole is closer to the optimal operating area than the other strategies. Since the end SOC of each strategy is approximately the same as the Figure 13, the Approximate-ECMS control conserves more energy.

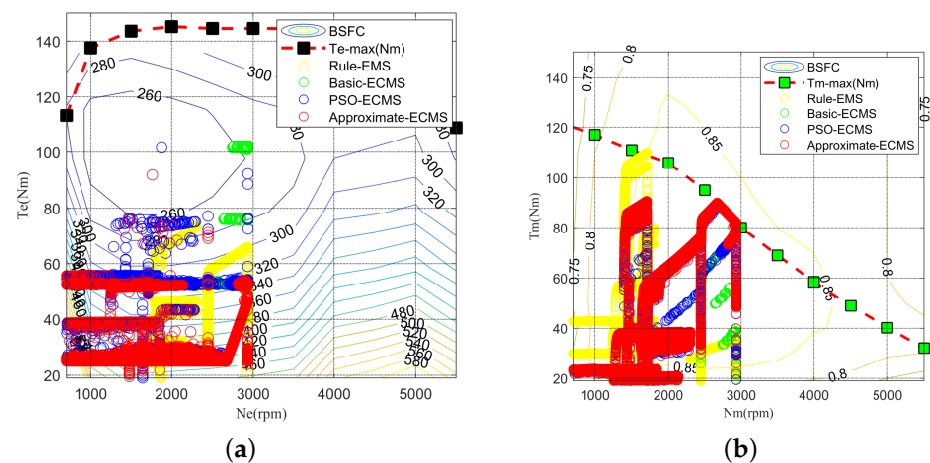


**Figure 14.** Operation points for (a) engine and (b) motor during NEDC driving cycle.

Table 3 shows the accumulated equivalent fuel consumption during the NEDC driving cycle. In the NEDC cycle, the final values of equivalent fuel consumption  $M_{eq}$  (L/km) under Rule-EMS, Basic-ECMS, PSO-ECMS, and Approximate-ECMS are [8.3876, 7.1443, 7.0884, 7.1354]. The comparison between Rule-EMS control and Approximate-ECMS resulted in a 17.55% improvement in fuel consumption  $M_e$  (L/km). It is apparent from this table that the PSO-ECMS is better than Basic-ECMS and Approximate-ECMS, which is due to the discretization increments in the online Basic-ECMS. The discretization increments of parameters are limited because of the simulation equipment such as the computer's CPU and memory. In summary, the Approximate-ECMS is more effective than Rule-EMS, Basic-ECMS, PSO-ECMS. However, the Approximate-ECMS is based on the fixed motor

efficiency and battery efficiency and the motor efficiency affects the results. Therefore, we move on to discussing the  $S_0$  next.

**Table 3.** Fuel consumption in the simulation of  $SOC_{init} = 0.7$  for NEDC driving cycle.

Strategy	$M_{eq}$ (L/km)	$M_e$ (L/km)	$M_{eq}$ Improved(%)
Rule-EMS	8.387	6.037	0
Basic-ECMS	7.144	4.793	17.40
PSO-ECMS	7.088	4.734	18.32
Approximate-ECMS	7.135	4.787	17.55

### 5.3. Optimization of $S_0$ Based on DPSO-GA

To compensate for the effect of changing motor efficiency on the result of Approximate-ECMS, DPSO-GA is used to optimize the initial equivalent factor  $S_0$ . We initialize particle swarm including swarm number 50 and the number of iterations of the hybrid DPSO-GA algorithm is set to 100 times.  $S_0$  is set to [0,4]. The energy consumption using optimization in NEDC is calculated and shown in Table 4 and Figure 15. The optimal  $S_0$  can improve the energy economy by 9.04% compared to the before optimization. From Figure 14, the final value of SOC is a little larger than before optimization, indicating that the engine is more involved in torque delivery. It is also clear that the engine operating point is close to the optimized region (240–280 g/kW h).

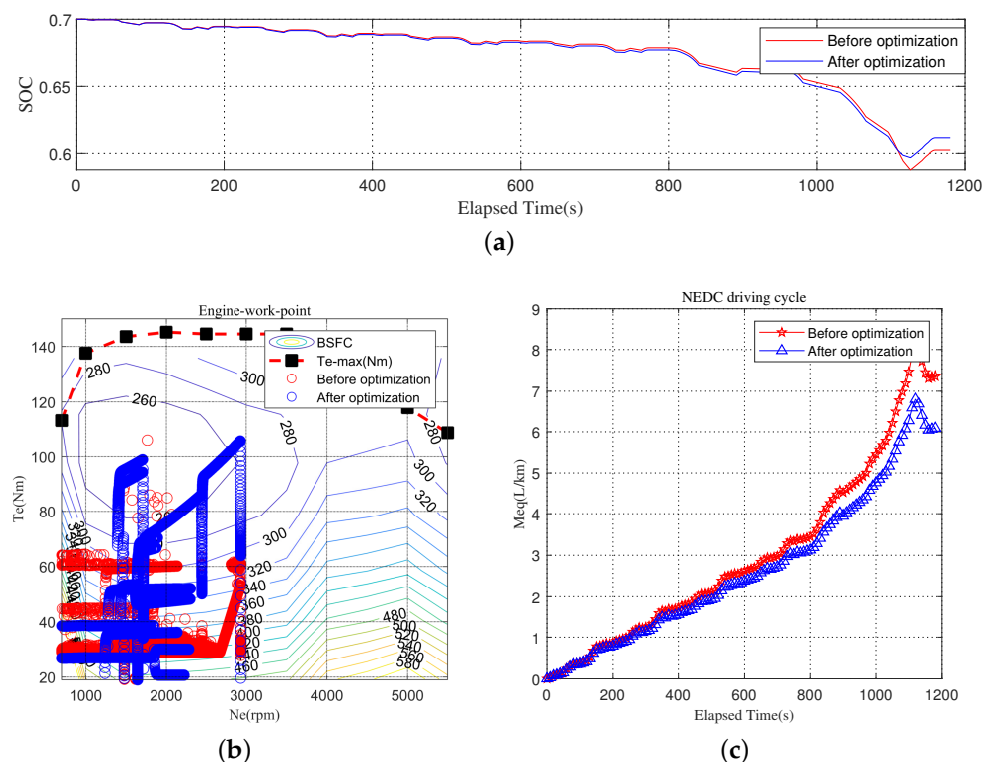


**Figure 15.** Comparison optimization during NEDC driving cycle. (a) SOC change trajectory. (b) Operation points for engine. (c)  $M_{eq}$  change trajectory.

**Table 4.** Comparison of optimization results.

	$S_0$	$M_{eq}$ (L/km)	$M_e$ (L/km)	$\Delta SOC$	$M_{eq}$ Improved
Before optimization	2.75	7.135	4.787	0.0541	0
After optimization	3.10	6.499	4.354	0.1205	9.04%

## 6. Conclusions

In this paper, Approximate-ECMS is proposed for real-time control under the single-shaft parallel hybrid powertrain, which considers both the fuel economy and computational load. Combined with the structural characteristics of the single-shaft parallel hybrid powertrain, the equivalent fuel consumption equation is fitted to the objective function by introducing the power allocation factor. Then it is solved numerically for candidate solutions to reduce computational load. To compensate for the effect of changing motor efficiency on the result of Approximate-ECMS, DPSO-GA is used to optimize the initial equivalent factor to obtain the best initial equivalence factor  $S_{opt}$  to improve the fuel economy for the NEDC driving cycle. The results show that the equivalent fuel consumption of Approximate-ECMS was 7.135 L/km by 17.55% improvement compared with Rule-ECMS in the New European Driving Cycle (NEDC). In addition, the results of Approximate-ECMS are close to Basic-ECMS and PSO-EMS. However, simulation time is faster than Basic-ECMS and PSO-EMS. This indicates that the Approximate-ECMS is an effective solution to optimize fuel economy and computational load for real-time control.

The accuracy improvement of fitting function is a crucial issue for improving control effects of Approximate-ECMS, which has been arranged in future directions. Furthermore, to adapt to different driving cycles, equivalence factor changes in real-time control should be considered to improve fuel economy. Last but not least, hardware-in-the-loop experiments and vehicle experiments can be performed to validate the effectiveness of the strategy in future research.

**Author Contributions:** H.Z. managed the conceptualized project. P.Q. designed the energy management strategy, completed the modeling and simulation, and wrote the manuscript. P.W. and T.P. collected the data. P.Q., H.Z. contributed to the validation and analysis of the results and reviewed the writing. All authors have read and agreed to the published version of manuscript.

**Funding:** Supported by National Natural Science Foundation of China (61573304).

**Conflicts of Interest:** The authors declare no conflict of interest.

## References

1. Qin, Y.; Tang, X.; Jia, T.; Duan, Z.; Zhang, J.; Li, Y.; Zheng, L. Noise and vibration suppression in hybrid electric vehicles: State of the art and challenges. *Renew. Sustain. Energy Rev.* **2020**, *124*, 109782. [[CrossRef](#)]
2. Tang, X.; Hu, X.; Yang, W.; Yu, H. Novel torsional vibration modeling and assessment of a power-split hybrid electric vehicle equipped with a dual mass flywheel. *IEEE Trans. Veh. Technol.* **2018**, *67*, 1990–2000. [[CrossRef](#)]
3. Wilberforce, T.; El-Hassan, Z.; Khatib, F.N.; Al Makky, A.; Baroutaji, A.; Carton, J.G.; Olabi, A.G. Developments of electric cars and fuel cell hydrogen electric cars. *Int. J. Hydrog. Energy* **2017**, *42*, 25695–25734. [[CrossRef](#)]
4. Xie, S.; Hu, X.; Liu, T.; Qi, S.; Lang, K.; Li, H. Predictive vehicle-following power management for plug-in hybrid electric vehicles. *Energy* **2019**, *166*, 701–714. [[CrossRef](#)]
5. Shi, D.; Wang, S.; Cai, Y.; Chen, L. Stochastic predictive energy management of power split hybrid electric bus for real-world driving cycles. *IEEE Access* **2018**, *6*, 61700–61713. [[CrossRef](#)]
6. Sun, X.; Diao, K.; Yang, Z.; Lei, G.; Guo, Y.; Zhu, J. Direct torque control based on a fast modeling method for a segmented-rotor switched reluctance motor in HEV application. *IEEE J. Emerg. Sel. Top. Power Electron.* **2019**, *99*, 1. [[CrossRef](#)]
7. Xu, N.; Kong, Y.; Chu, L.; Ju, H.; Yang, Z.; Xu, Z.; Xu, Z. Towards a smarter energy management system for hybrid vehicles: A comprehensive review of control strategies. *Appl. Sci.* **2019**, *9*, 2026. [[CrossRef](#)]
8. Liang, J.; Li, Y.; Jia, W.; Lin, W.; Ma, T. Comparison of Two Energy Management Strategies Considering Power System Durability for PEMFC-LIB Hybrid Logistics Vehicle. *Energies* **2021**, *14*, 3262. [[CrossRef](#)]
9. Zhou, H.; Xu, Z.; Liu, L.; Liu, D.; Zhang, L. A rule-based energy management strategy based on dynamic programming for hydraulic hybrid vehicles. *Math. Probl. Eng.* **2018**, *2018*, 10. [[CrossRef](#)]
10. Tang, X.; Yang, W.; Hu, X.; Zhang, D. A novel simplified model for torsional vibration analysis of a series-parallel hybrid electric vehicle. *Mech. Syst. Sig. Process* **2017**, *85*, 329–338. [[CrossRef](#)]
11. Jiang, Q.; Ossart, F.; Marchand, C. Comparative study of real-time HEV energy management strategies. *IEEE Trans. Veh. Technol.* **2017**, *66*, 10875–10888. [[CrossRef](#)]
12. Ali, A.M.; Söffker, D. Towards optimal power management of hybrid electric vehicles in real-time: A review on methods, challenges, and state-of-the-art solutions. *Energies* **2018**, *11*, 476. [[CrossRef](#)]
13. Zhuang, W.; Zhang, X.; Li, D.; Wang, L.; Yin, G. Mode shift map design and integrated energy management control of a multi-mode hybrid electric vehicle. *Appl. Energy* **2017**, *204*, 476–488. [[CrossRef](#)]

14. Pérez, L.V.; Bossio, G.R.; Moitre, D.; García, G.O. Optimization of power management in a hybrid electric vehicle using dynamic programming. *Math. Comput. Simul.* **2006**, *73*, 244–254. [[CrossRef](#)]
15. Sun, X.; Hu, C.; Zhu, J.; Wang, S.; Zhou, W.; Yang, Z.; Guo, Y. MPTC for PMSMs of EVs with multi-motor driven system considering optimal energy allocation. *IEEE Trans. Magn.* **2019**, *55*, 8104306. [[CrossRef](#)]
16. Li, L.; Yang, C.; Zhang, Y.; Zhang, L.; Song, J. Correctional DP-based energy management strategy of plug-in hybrid electric bus for city-bus route. *IEEE Trans. Veh. Technol.* **2015**, *64*, 2792–2803. [[CrossRef](#)]
17. Peng, H.; Li, J.; Deng, K.; Thul, A.; Li, W.; Lowenstein, L.; Sauer, D.U.; Hameyer, K. An Efficient Optimum Energy Management Strategy Using Parallel Dynamic Programming for a Hybrid Train Powered by Fuel-Cells and Batteries. In Proceedings of the 2019 IEEE Vehicle Power and Propulsion Conference (VPPC), Hanoi, Vietnam, 14–17 October 2019; pp. 1–7.
18. Du, G.; Zou, Y.; Zhang, X.; Liu, T.; Wu, J.; He, D. Deep reinforcement learning based energy management for a hybrid electric vehicle. *Energy* **2020**, *201*, 117591. [[CrossRef](#)]
19. Ferrario, A.M.; Manzano, F.S.; Bocci, E. Hydrogen vs. Battery in the Long-term Operation. A Comparative Between Energy Management Strategies for Hybrid Renewable Microgrids. *IEEE Consum. Electron. Mag.* **2020**, *9*, 1–28.
20. Yao, Z.; Wang, Y.; Liu, B.; Zhao, B.; Jiang, Y. Fuel consumption and transportation emissions evaluation of mixed traffic flow with connected automated vehicles and human-driven vehicles on expressway. *Energy*, **2021**, *230*, 120766. [[CrossRef](#)]
21. Paganelli, G. Conception et commande d'une chaîne de traction pour véhicule hybride parallèle thermique et électrique. Ph.D. Thesis, Hauts-de-France Polytechnic University, Valenciennes, France, 1999.
22. Geng, B.; Mills, J.K.; Sun, D. Energy management control of micro turbine-powered plug-in hybrid electric vehicles using the telemetry equivalent consumption minimization strategy. *IEEE Trans. Veh. Technol.* **2011**, *60*, 4238–4248. [[CrossRef](#)]
23. Gao, A.; Deng, X.; Zhang, M. Design and validation of real-time optimal control with ECMS to minimize energy consumption for parallel hybrid electric vehicles. *Math. Probl. Eng.* **2017**, *2017*, 1–13. [[CrossRef](#)]
24. Hou, C.; Ouyang, M.; Xu, L.; Wang, H. Approximate Pontryagin's minimum principle applied to the energy management of plug-in hybrid electric vehicles. *Appl. Energy* **2014**, *115*, 174–189. [[CrossRef](#)]
25. Rezaei, A.; Burl, J.; Zhou, B. Estimation of the ECMS equivalent factor bounds for hybrid electric vehicles. *IEEE Trans. Control Syst. Technol.* **2018**, *26*, 2198–2205. [[CrossRef](#)]
26. Guo, S.; Dang, C.; Liao, X. Joint opportunistic power and rate allocation for wireless ad hoc networks: An adaptive particle swarm optimization approach. *J. Netw. Comput. Appl.* **2011**, *34*, 1353–1365. [[CrossRef](#)]
27. Alfi, A.; Modares, H. System identification and control using adaptive particle swarm optimization. *Appl. Math. Model.* **2011**, *35*, 1210–1221. [[CrossRef](#)]
28. Wu, X.; Cao, B.; Wen, J.; Bian, Y. Particle swarm optimization for plug-in hybrid electric vehicle control strategy parameter. In Proceedings of the IEEE Vehicle Power and Propulsion Conference, Harbin, China, 3–5 September 2008.
29. Chen, Z.; Xiong, R.; Cao, J. Particle swarm optimization-based optimal power management of plug-in hybrid electric vehicles considering uncertain driving conditions. *Energy* **2016**, *96*, 197–208. [[CrossRef](#)]
30. Wang, Y.; Wang, X.; Sun, Y.; You, S. Model predictive control strategy for energy optimization of series-parallel hybrid electric vehicle. *J. Clean. Prod.* **2018**, *199*, 348–358. [[CrossRef](#)]
31. Chen, S.Y.; Wu, C.H.; Hung, Y.H. Optimal Strategies of Energy Management Integrated with Transmission Control for a Hybrid Electric Vehicle using Dynamic Particle Swarm Optimization. *Energy* **2018**, *160*, 154–170. [[CrossRef](#)]
32. Hwang, H.-Y.; Chen, J.-S. Optimized Fuel Economy Control of Power-Split Hybrid Electric Vehicle with Particle Swarm Optimization. *Energies* **2020**, *13*, 2278. [[CrossRef](#)]
33. Ferrario, A.M.; Bartolini, A.; Manzano, F.S. A model-based parametric and optimal sizing of a battery/hydrogen storage of a real hybrid microgrid supplying a residential load: Towards island operation. *Adv. Appl. Energy* **2021**, *3*, 100048. [[CrossRef](#)]
34. Tian, X.; He, R.; Sun, X.; Cai, Y.; Xu, Y. An ANFIS-based ECMS for Energy Optimization of Parallel Hybrid Electric Bus. *IEEE Trans. Veh. Technol.* **2019**, *69*, 1473–1483. [[CrossRef](#)]
35. Xie, S.; Hu, X.; Xin, Z.; Brighton, J. Pontryagin's minimum principle based model predictive control of energy management for a plug-in hybrid electric bus. *Appl. Energy* **2019**, *236*, 893–905. [[CrossRef](#)]
36. Lin, X.; Feng, Q.; Mo, L.; Li, H. Optimal adaptation equivalent factor of energy management strategy for plug-in CVT HEV. *Proc. Inst. Mech. Eng. Part D J. Automob. Eng.* **2019**, *233*, 877–889. [[CrossRef](#)]
37. Lei, Z.; Qin, D.; Hou, L.; Peng, J.; Liu, Y.; Chen, Z. An adaptive equivalent consumption minimization strategy for plug-in hybrid electric vehicles based on traffic information. *Energy* **2020**, *190*, 116409. [[CrossRef](#)]
38. Assareh, E.; Behrang, M.A.; Assari, M.R.; Ghanbarzadeh, A. Application of PSO (particle swarm optimization) and GA (genetic algorithm) techniques on demand estimation of oil in Iran. *Energy* **2010**, *35*, 5223–5229. [[CrossRef](#)]
39. Song, Z.; Wu, G.; Zheng, S. Multi-objective optimization of energy management strategy of plug-in hybrid electric vehicle. *J. Tongji Univ.* **2011**, *39*, 99–103.
40. Guo, Q.; Zhao, Z.; Shen, P.; Zhan, X.; Li, J. Adaptive optimal control based on driving style recognition for plug-in hybrid electric vehicle. *Energy* **2019**, *186*, 115824. [[CrossRef](#)]